Optical Component Analysis for Ultrahigh Concentrated Photovoltaic System (UHCPV)

Mussad Alzahrani[1, 2*], Asmaa Ahmed[1, 3], Katie Shanks[1], Senthilarasu Sundaram[1], Tapas Mallick[1]

[1]Environmental and Sustainability Institute, University of Exeter, Penryn, UK TR10 9FE

[2]Mechanical and Energy Engineering Department, Imam Abdulrahman Bin Faisal University, Dammam, 34212, Saudi Arabia

[3]Mechanical Power Engineering Department, Port Said University, Port Said 42523, Egypt

*Corresponding author: ma778@exeter.ac.uk

Abstract

This article investigates the discrepancy between the theoretical and the experimental optical characterisation results of a Fresnel Lens - silicon on glass (SOG), as a primary optical component toward UHCPV of > 3000 suns design (Shanks et al., 2018). All the equations were elaborated for single- and multi-junction solar cells, emphasising the performance when the focal spot area is larger or lesser than the solar cell area. This simple prediction approach of optical characterisation has shown a strong agreement between the theoretical and experimental results of the multi-junction solar cell with a discrepancy of 2% at 7.7 W (77 suns) and 6% on the average cross a solar irradiance on the cell from 3.1W – 7.7 W corresponding to 31 suns – 77 suns in concentration ratio. A theoretical analysis of the optical performance for a 1/4 of the system grouping three optical interfaces is performed to estimate the optical loss and its influence on the optical efficiency and optical concentration ratio.

Keywords: Fresnel lens, multi-junction solar cell, UHCPV, optical efficiency, solar concentrator.

Nomenclature

J	Radiant Flux ($\frac{W}{m^2}$).
C	Concentration Ratio (Sun)
A	Area (m^2)
$\%T$	Total transmittance (%)
%C	Fractional Loss (%)
I	Current (mA)
V	Voltage (mV)

Greek Symbols

η	Effecieny (%)

Subscript

g	Geometrical
th	Theoretical
Opt	Optical
Fresenl	Fresenl lens
Receiver	Receiver area of the solar cell
eff	Effective
Si	Silicon
oc	Open circuit
sc	Short circuit
exp	Experimental
T	Top
M	Middle

Abbreviations

UHCPV	Ulterhigh concetration ratio
CPV	Concentrated photovoltaic
MJ	Multi-junction
1J	Single – junction
FF	Fill factor
UV	Ultraviolet
SOG	Silicon on Glass
CCD	charged-coupled device

1. Introduction

The need for solar energy and its application is growing; however, the current solar PV technology is limited by its cost-effectiveness and power density due to space limitations (M. Alzahrani et al., 2021b). There is also a growing concern about the environmental impact of the materials utilised for solar PV (Tawalbeh et al., 2021). To overcome these drawbacks, the concentrated photovoltaic system (CPV) intends to replace the usage of a large number of PV panels with inexpensive optics to intensify sun rays into smaller solar cells. Ultrahigh concentrator photovoltaic (UHCPV) has a high potential to increase the power output and minimise the solar cell size, which lowers the cell cost and upsurges the competitiveness of the CPV system. The ultrahigh concentration ratio is achieved by integrating multiple optics in one system. The succession of optics in the CPV system is designed to concentrate the incoming sun rays where the quality and shape of an optical surface strongly influence the optical losses. To achieve the ultrahigh level, the sunlight divergence should be abated to intensify the solar irradiance within a relatively small acceptance angle, considering the limitation by the angular size of the sun and submits to the law of etendue conservation. The concentrator optics performance evenly relies on the manufacturing criteria, such as optics thickness and surface smoothness. The ultrahigh CPV system required a super-accurate tracking system to ensure minimal light divergence. The weight of optics and overall system components need to be carefully evaluated and interlinked with the payload design condition of a tracking system to ensure excellent solar monitoring and avoid tracking errors and dynamic load impact. An excellent optical tolerance allows room

for relatively small misalignment during the stage of manufacturing and operation (Daneshazarian et al., 2018; Sharaf and Orhan, 2015). There is continually an unavoidable correlation among acceptance angle, optical efficiency and irradiance distribution but options were given to enhance those criteria (Shanks et al., 2016). Optics, such as light funnels and homogenisers, have been applied to relatively uniform the solar irradiance on the receiver area and to enlarge the acceptance angle (Canavarro et al., 2013; Fu et al., 2010; Gordon et al., 2008; Tang and Liu, 2011; Tang and Wang, 2013; Winston et al., 2005). Also, the reflective secondary optical stage has been introduced into the CPV system to enhance the solar flux distribution. However, incorporating those optics within the CPV system can decrease the optical efficiency and hence the concentration ratio due to their optical performance. Out of these, the attention to the elevated temperature on the subsequent optics after the primary optic and the receiver is most considered to avoid any thermo-mechanical stresses as a result of intensified solar irradiance. The solar cells should be maintained below 80 ℃ to act electrically within its safe operating conditions (Alzahrani et al., 2020). Thus, the optical tolerance in UHCPV required an investigation for all possible alignment uncertainty and losses, and that is unachievable without compromising with optical efficiency, concentration ratio, irradiance distribution, and the solar cell electrical performance.

Based on the concentration factor (sun), the CPV system is classified as either a low concentrated photovoltaic system (LCPV) (suns < 10), as a medium concentrated photovoltaic system (MCPV) (10 < suns <100), as a high concentrated photovoltaic system (HCPV) (100 < suns < 2000), and as an ultrahigh concetrated photovoltaic system (UHCPV) (suns >2000) (M. Alzahrani et al., 2021b; Shanks et al., 2016). As moving toward a higher concentration factor, the subsequent optics to the primary optic is exposed to a relatively higher temperature range to reach its maximum concentration and hence temperature on the solar cell.

The process of thermal extrication in a CPV system depends on the concept of either a pre-illumination cooling mechanism based on spectral decomposition or a post-illumination cooling mechanism based on heat transfer fluid (HTF). Post-illumination cooling is a common technique and well developed through either passive or active mechanisms. The active cooling mechanism proved its capability in maintaining the solar cell temperature; however, there is a parasitic load proportional correlation with increasing the concentration ratio where more fluid is needed to be pumped or fanned through the heat dissipation domain. Interestingly, two papers discussed a passive flat-plate heatsink's performance (AlFalah et al., 2020; Valera et al., 2019) and different microscale pin-fin configurations for a concentration ratio of up to 10000 suns. The last study found that the linking of a microscale pin-fin with a flat-plate heatsink can operate the solar cell safely to 12000 suns but only with the solar cell size not exceeding $1 \times 1\ mm^2$. Although the achieved level of concentration ratio is promising, such a cell size will certainly impede the system alignments and tracking accuracy.

The pre-illumination cooling mechanism directs the matchable spectral wavelength band to the solar cell and rejects or redirects the unutilised wavelength band to a thermal receiver. The difficulties in matching the optical properties with either the optical decomposition filter or HTF reflects the less maturation of the pre-illumination cooling mechanisms. The optical filter transmits a selective segment of the optical wavelength while eliminating other wavelength segments through multiple optical filtering techniques. Recently, one of these optical techniques, termed a “neutral density filter (ND)”, was adopted as a pre-illumination cooling mechanism based on graphene material to attenuate the intensity of the solar irradiance for a CPV system (M. Alzahrani et al., 2021a; M. M. Alzahrani et al., 2021).

Increasing the concentration ratio results in inducing the temperature to a level at which the electrical performance is degraded. The state-of-the-art multi-junction solar cells exhibit a drop in cell efficiency for concentrations above a specific value due to their resistive losses. As a result, cooling arrangements is crucial in CPV system for consistent solar efficiency performance. A future solar cell architecture has been investigated for energy harvesting in the ultrahigh concentration range. Fernández et al. (Suns et al., 2019) developed a Vertical-tunnel-junction (VTJ) solar cell that showed no degradation in cell efficiency of 28.4 % with a concentration ratio of up to 15,000 suns. El-Gahouchi et al. (El-Gahouchi et al., 2020) fabricated duplicated junction solar cell architectures that can produce electrical energy with 33% of cell efficiency at 3,500 suns and 28% of cell efficiency beyond 10,000 suns.

Cassegrain-based and Fresnel-based focal point designs have been developed to reach ultrahigh concentration ratio design with high performance. For Cassegrain-based, Ferrer-rodríguez et al. (Ferrer-Rodríguez et al., 2016) designed an optical configuration of 4-off-axis Cassegrain ultrahigh concentrator photovoltaic module where it has a geometrical concentration ratio of 2304x. For this design, the effective optical efficiency, as the proportion between the power concentrated on the solar cell to the incoming module power, is 73% resulting in an effective optical concentration ratio of 1682 suns. Dreger et al. (Dreger et al., 2014) configured a mini-Cassegrain mirror optics concentrators to achieved a geometrical concentration ratio of 1037x. Still, due to the primary and secondary optics shape deviations, the effective optical efficiency is 77% resulting in the effective concentration ratio of 800 suns. In any case, paraboloid-hyperboloid pairs of optics have high surface roughness, and the polishing for the conical-shaped would alter the curvature and introduce optical inaccuracies in directing and redirecting of sun rays. Thus, for Fresnel-based, Miñano et al. (Miñano et al., 2013) has investigated the Fresnel lens theoretically toward the ultrahigh concentration ratio level. Dome-shaped Fresnel lens has been configured

with four entrances into an optical receiver. This design has a geometrical concentration ratio of 2300x. Still, due to imperfection in the reflective and refractive optics and front metalised area on the secondary optics, the optical efficiency is 82% resulting in the optical concentration ratio of 1897suns. The manufacturability of the domed Fresnel lens is difficult and expensive due to the need for a unique casting mould. Thus, Shanks et al. (Shanks et al., 2018) investigated an ultrahigh Fresnel lenses design based on 4- flat Fresnel Lens (SOG) concentrating into one central receive with the existence of redirecting optical materials has shown a geometrical and optical concentration ratio of 5831x and 4373 suns, respectively. In this design, a flat mirror as a secondary optics were selected instead of conically shaped due to its low surface roughness. Also, the favorability of the flat mirror is due to easy manufacturability and employability of reflective film (~ 97%) at a relatively low cost.

Fresnel lens is a refractive optical component that converges input solar rays into a focal spot. The focal length is idealised based on the intercept radius by readjusting the Fresnel lens position for its optimum energy output. Fresnel lens is one of the common primary concentrators in concentrator photovoltaic (CPV) system for its cost-effective, lightweight, relatively high acceptance angle and optical efficiency. However, the standard Fresnel lens is limited in concentration ratio to about 1000 suns due to the alteration of its refractive index materials with temperature (chromatic aberration). Thus, achromatic Fresnel doublets show a minimised chromatic aberration, increasing the concentration factor (González Montes et al., 2014; Shanks et al., 2016). Experimentally, a flat achromatic fresnel doublet showed a concentration factor of up to 2000x but is still not commercially available (Languy et al., 2013). Silicon-on-glass (SOG) Fresnel lens is manufactured by applying a thin layer of liquid silicon into a glass. The stamping and curing process is performed to form the Fresnel structure. However, the thin silicon layer leads to strong dependence between the ambient temperature and optical efficiency at which the thermal expansion coefficient of the silicon to glass magnitude is different. Thus, the temperature effect hinders the optical efficiency for the Fresnel lens and the solar cell efficiency due to different focal lengths and focal spot sizes(Hornung et al., 2011).

Optical characterisation of a Fresnel lens was found in the literature, mostly analysing the irradiance distribution of the focal spot for energy and optical efficiency with demanding approaches. Chemisana et al. (Chemisana et al., 2011) established an experimental practice on the performance of the Lambertian source (opal diffuser) is conducted to optically characterised Fresnel lenses. This practice relies on CCD Camera to capture the concentrated solar irradiance profile over the opal diffuser. Optical characteristics components such as optical efficiency and concentration ratio in the concentrated area on the receiver have been acquired for linear- and point-focus Fresnel lens.

Sansoni et al.(Sansoni et al., 2007) examined different patterns of the prismatic lens with different materials on the basis of the optical project. This adopted approach aims to prove the resemblance between the collector's theoretical design and the prismatic lens's performance. To do so, four different mask shapes, a collimator mirror, and concentrator mirror, photodetector, and integrated sphere are needed to attain optical characteristics through testing for the total collection efficiency, for the energy distribution evaluation, and the uniformity estimation.

Martinez Antón et al.(Martinez Antón et al., 2011) conducted another method to characterise the Fresnel lens flux transfer performance. This method depends on suiting the camera's entrance focus at the focal spot at which the camera image gives detailed performance maps of the variety of Fresnel lenses for different acceptance angles. The captured maps allow an estimation of the overall optical efficiency and demonstrate the error and defects of the refractive concentrator. This characterisation method is challenged by increasing the working area of the Fresnel lens, where the flux performance deteriorates significantly.

Victoria et al. (Victoria et al., 2016) showed a characterisation method anticipated by the IES-UPM to measure the optical efficiency and irradiance distribution generated by silicon-on-glass (SOG) and PMMA Fresnel lens. This method required a solar cell of a large area (for optical efficiency measurements) and a CCD camera with a low- or high-pass filter plus a diffuser (for irradiance distribution and focal spot size). A top and middle subcells were used for the optical efficiency measurements at which the short-circuit current (I_{sc}) is determined for each subcell of the multi-junction solar cell.

Further, Wang et al.(Wang et al., 2018) studied the optical performance of a Fresnel lens based on the polar-axis tracking system. The results show that the maximum optical efficiency loss experimentally is 1.87%. The maximum possible tracking error is 1°, where 1.5° of tracking error results in an optical efficiency loss of 17.42%. Wiesenfarth et al. (Wiesenfarth et al., 2014) considered the influence of the solar spectrum and the solar cell spectral response in optical characterisation but not for an ultrahigh concentration ratio and similar size Fresnel lens.

In this study, we show that simple measurements and geometrical calculations can be used to give a close prediction of the optical efficiency and concentration ratio instead of using complicated and time-consuming ray trace analysis. To experimentally measure the optical products (optical efficiency and concentration ratio), a single-junction solar cell of $10 \times 10\ mm^2$ and $5.1 \times 5.1\ cm^2$ and a multi-junction solar cell of $10 \times 10\ mm^2$ are examined to compare with the theoretical analysis taking into consideration the geometrical calculations for the discrepancy determinations. This is an advantageous way to characterise the primary optic performance and move onto the more challenging secondary and tertiary optic characterisations for ultrahigh concentration. Hence,

outlines for the equations' details of the theoretical optical efficiency and concentration ratio and of the effective optical efficiency and concentration ratio with the fractional concentration loss and its influence on the optical characterisation are explicitly illustrated. In addition, a full theoretical analysis of the UHCPV system is considered for different receiver sizes, dissimilar coatings materials on the reflective mirrors-secondary optic stage, and the tertiary optic.

2. Primary optic assessment/analysis – Fresnel Lens

2.1. Theoretical optical characterisation

Two single junctions Polycrystalline silicon solar cell; one of $10 \times 10\ mm^2$ surface area and the another of $5.1 \times 5.1\ cm^2$surface area, manufactured by SUNYIMA and one $10 \times 10\ mm^2$ multi-junction solar cell with base material of GaInP/GaInAs/Ge on Ge substrates manufactured by AzurSppace (Azur Space Solar Power GMBH, 2014) are electrically investigated with and without a Fresnel lens as a refractive optical concentrator whilst maintaining the temperature of the back surface with a cooling mount base. The solar simulator manufactured by WACOM [Model no. WXS-210S-20] incorporates Xenon short-arc lamp and UV filter and AM 1.5G filter to emulate a solar irradiance approximating AM 1.5G. This solar simulator is rated as class AAA and has a spatial non-uniformity of solar irradiance within $\pm 2\%$. The used solar simulator coincides significantly with the AM 1.5G solar spectrum at 1000 W/m^2, as in Figure 1. We have tested the cells under AM 1.5G spectrum with a beam divergence of 1.43°, which is not the standard test condition for the multi-junction solar cells, but this helps indicates the worst-case scenario values for the system before moving for outdoor testing.

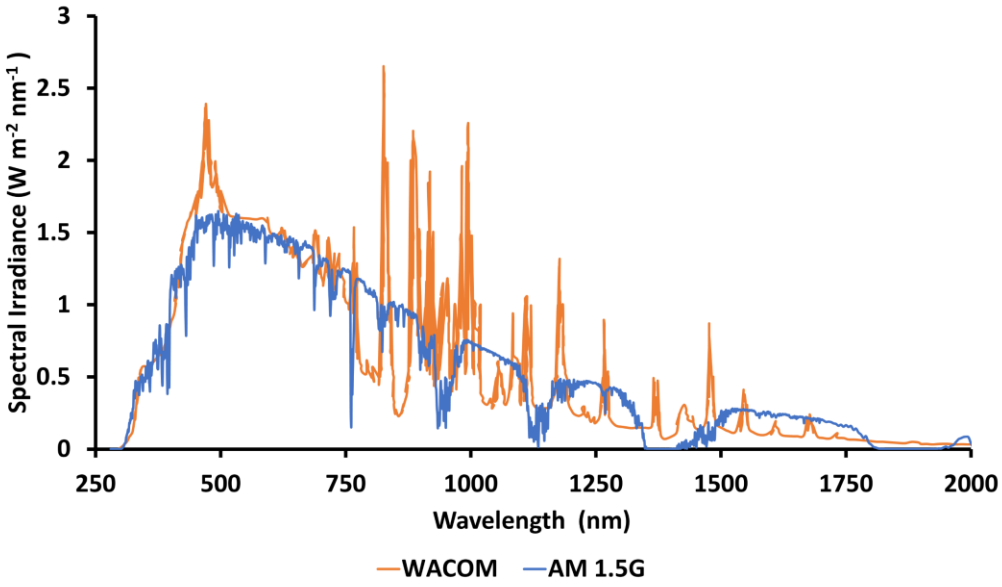

Figure 1 The solar spectrum profile for the used WACOM solar simulator with AM 1.5G.

The External Quantum efficiency (EQE) (%) was measured for the multi-junction solar cells and the polycrystalline Si solar cells to define the number of electrons out per incident photon. EQE was calculated for a wavelength compatible with the cells using Bentham PVE300 PV characterisation setup under standard AM 1.5 solar spectrum, as in Figure 2.

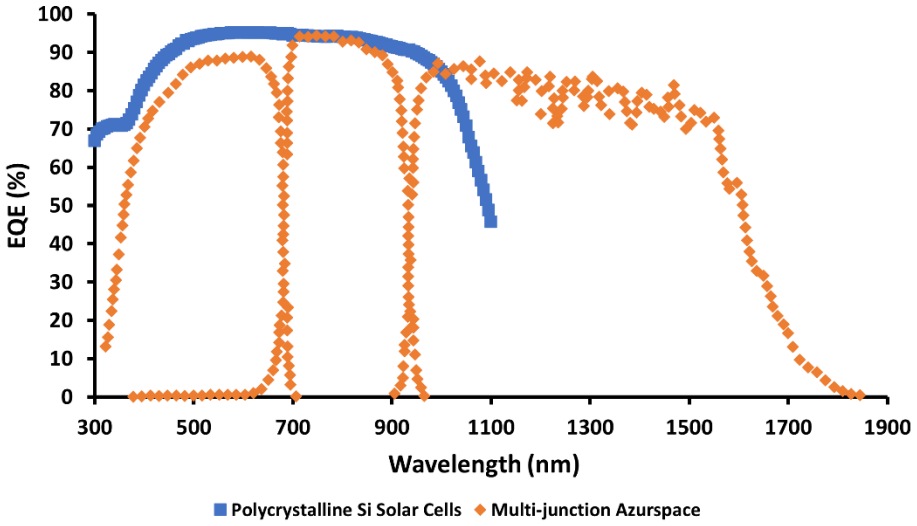

Figure 2 EQE (%) measurements for the multi-junction solar cells and the polycrystalline Si solar cells.

Silicon on glass (SOG) Fresnel lens of aperture area of 529 cm^2 (23 cm × 23 cm) manufactured by ORAFOL based on untempered low-iron float glass has been introduced under the solar simulator and adjusted in height for the optimum focal spot and length where the highest concentration ratio is achieved. The irradiance output from a Fresnel lens is typically Gaussian distribution in contour (Jing et al., 2012). However, this Fresnel lens has an excellent relatively uniformed output over at least 1 cm in the centre. The solar cells have been placed within the focal spot and aligned for maximum electrical generation. However, within the focal spot, temperature raises significantly due to the high concentration ratio. So, to avoid any thermomechanical defects to the solar cell and to assure a good fill factor (FF), a cooling mount setup is introduced at 25 °C, as in Figure 3. Temperature is observed during the experiment utilising a thermocouple meter (Datalogger SDL200 - EXTECH INSTRUMENTS) to establish safe operating conditions.

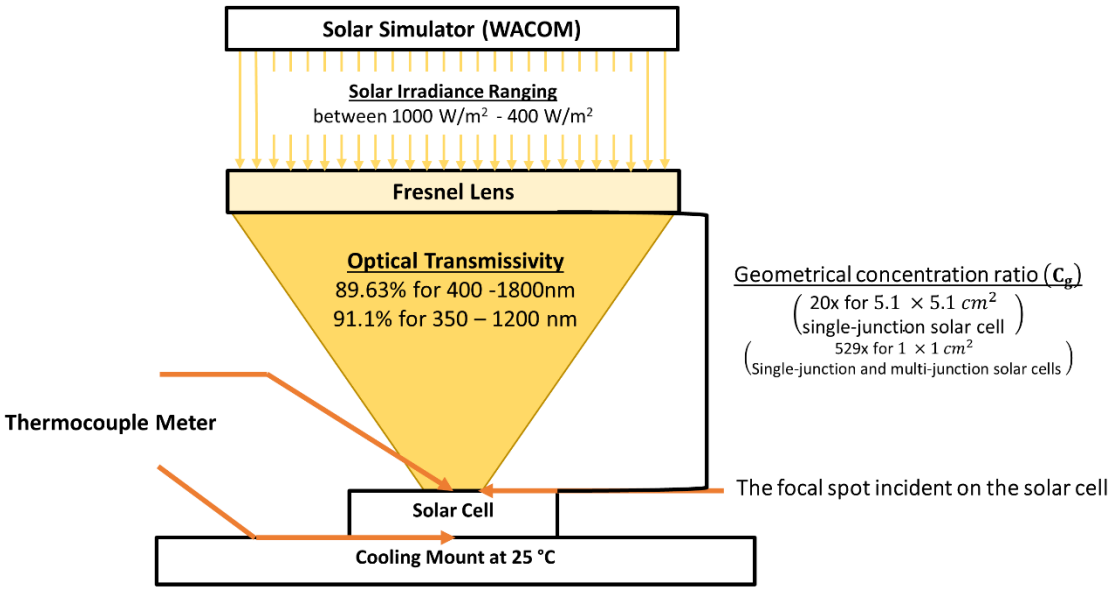

Figure 3 Schematic diagram describing the experimental setup where AM 1.5G was simulated by WACOM solar simulator manufacturers ("WACOM ELECTRIC LTD," 2021).

A spectrophotometer device (PerkinElmer) is used to measure the total transmittance of the Fresnel lens (SOG) to allow accurate analysis for the optical efficiency and concentration ratio over the multi-junction and single-junction solar cells wavelength response range between 400 – 1800 nm and 350 – 1200 nm, respectively. The measured total transmittance will help to find out the optical efficiency and the concentration ratio of the Fresnel lens, which is intended to be 1 of 4 primary lenses in the ultrahigh CPV version of the system (Shanks et al., 2018).

To theoretically characterise the optical efficiency ($\eta_{opt,th}$) and the concentration ratio (C_{th}), we incorporate the average total transmittance ($\%T$), the geometrical concentration ratio (C_g), and the fractional concentration loss ($\%C$) with radiant flux (J) on the receiver area ($A_{receiver}$), and then divided with the radiant flux on the concentrator area ($A_{Fresnel}$), as in Eq.1. For the multi-junction solar cell, the influence of incident spectrum irradiance on the short-circuit current (I_{sc}) to determine the photocurrent generation ratio of the top subcell over the middle subcell (I_T/I_M) should be accountable for in the calculation of the optical efficiency (Fernández, E.F., Almonacid, F., Rodrigo, P.M., Pérez-Higueras, 2017; Muñoz-Cerón et al., 2012). I_T/I_M terms in Eq.1 is only to express that the optical efficiency for the case of a multi-junction cell is driven by the photocurrent generation ratio.

$$\boldsymbol{\eta_{opt,th}} = \frac{(\mathrm{J}\times \boldsymbol{A_{receiver}})\times \%\boldsymbol{T}\times \boldsymbol{C_g}\times \%\boldsymbol{C}}{(\boldsymbol{J}\times \boldsymbol{A_{Fresnel}})} \times \frac{I_T}{I_M} \quad (1)$$

Hence, the theoretical concentration ratio can be given by Eq.2.

$$\boldsymbol{C_{th}} = \boldsymbol{\eta_{opt,th}} \times \boldsymbol{C_g} \quad (2)$$

The adjustment of the Fresnel lens under the solar simulator at 1000 W/m^2 shows an optimum focal length and a focal spot of $\sim 42\ cm$ and $2.8\ cm$, respectively. Figure 4 shows the experimental setup under the solar simulator and the tested solar cells.

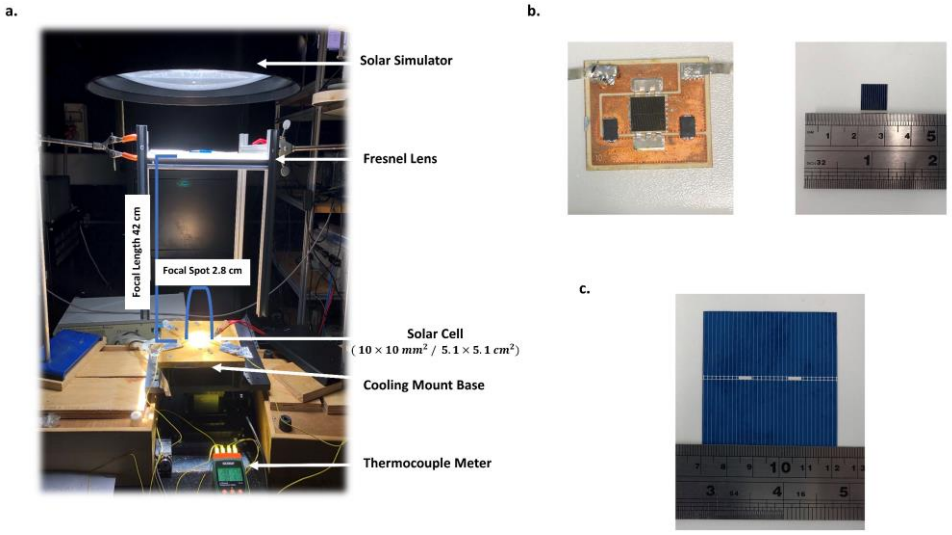

Figure 4 a. Lab experimental setup for the primary optical components. b. Azur Space 3C44A (10×10 mm^2)and Si polycrystalline single junction (10×10 mm^2). c. Si polycrystalline single-junction (5.1×5.1 cm^2)

The optical efficiency and optical concentration ratio after the Fresnel lens and with fractional concentration loss in preliminary setup are given with the wavelength range as well as two theoretical scenarios of optical efficiency, standard at 55% and state-of-art at 75% as in (Shanks et al., 2018) and in Figure 5. The two scenarios demonstrate a further understanding of the optical efficiency and concentration ratio losses by incorporating multiple optical interfaces or optics with poor performance.

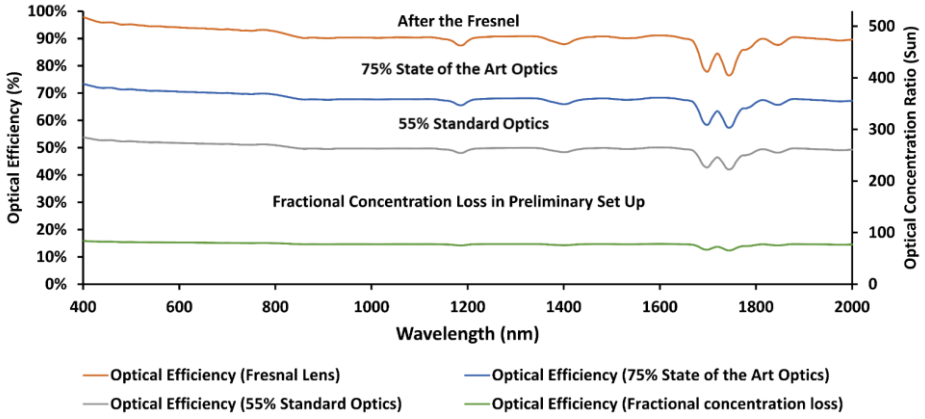

Figure 5 Theoretical optical efficiency and optical concentration ratio with wavelength (computed relying on a solar cell area of 10×10 mm^2 as a final stage)

Clearly, the theoretical optical concentration ratio has shown a drop-in comparison to the geometrical concentration ratio on average by 10% for after the Fresnel lens. Also, the theoretical concentration ratio has shown a drop in contrast to after the Fresnel lens on average to be 25%, 45% and 84% for 75% state of the art optics, 55% standard optics and fractional concentration loss in preliminary setup, respectively. The theoretical concentration ratio considering the fractional loss was found to be 77 suns on average.

The theoretical effective concentration ratio ($C_{eff,th}$) is calculated as the actual solar irradiance on the solar cell surface area after transmitting and concentrating through the Fresnel lens at different solar irradiance in the range of 400-1000 W/m^2 given the theoretical optical efficiency, as in Eq. 3:

$$\boldsymbol{C_{eff,th}} = \frac{\boldsymbol{J \times C_g \times \eta_{opt,th}}}{\boldsymbol{1000}} = \frac{\boldsymbol{J \times A_{Fresnel} \times \%T}}{\boldsymbol{A_{receiver} \times 1000}} \quad (3)$$

2.2. Experimental optical characterisation

The optical characterisation of the Fresnel lens is experimentally achievable through the electrical characterisation of a solar cell. Indoor, we can control the solar intensity of the lamp (helicon value) at which electrical characterisation for different solar irradiance (concentration ratio after the Fresnel) is realistic. We simulate the solar irradiance from 400 – 1000 W/m^2 in the interval of 100 W/m^2 to measure the solar cell electrical products (I_{sc} , V_{oc}, FF). The I-V and power curves for the multi-junction solar cell (Azur Space 3C44A 10×10 mm^2), for Si polycrystalline single-junction (10×10 mm^2), and Si polycrystalline single-junction (5.1 × 5.1 cm^2) are measured to determine the electrical limits with and without the Fresnel lens. The optimum arrangement of the Fresnel lens results in focal spot utilisation by the solar cell of 10×10 mm^2 of only 16.24%, which is the actual portion of light falling on the cell, resulting in optical efficiency of 14.6% (Fractional concentration efficiency of 16.24% × average Fresnel lens transmittance of 89.6%) and concentration ratio of 77 suns, as illustrated in Figure 6.a. In a solar cell of 5.1 × 5.1 cm^2, the solar cell area is more significant than the focal spot area; hence the geometrical concentration ratio (the Fresnel lens area divided by the solar cell area) is not quite appropriate and instead the Fresnel input aperture area divided by the illuminated cell area would give a more useful indication of concentration ratio. In Figure 6.b, the theoretical optical efficiency was found to be 91.1% (simply the Fresnel transmittance), resulting in a theoretical concentration ratio of 18 suns.

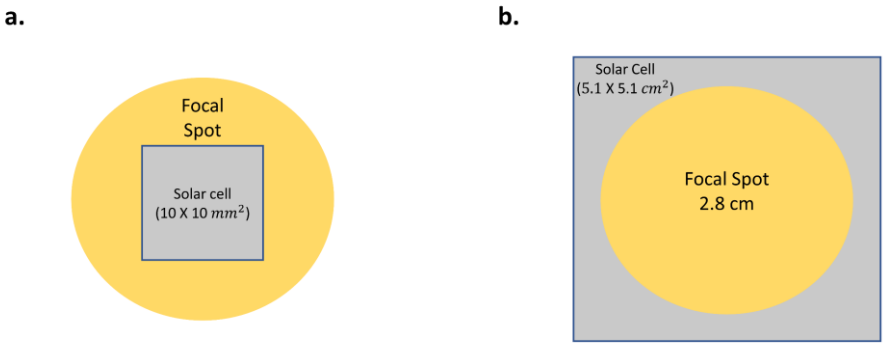

Figure 6 a schematic diagram of a. fractional concentration loss (solar cell to focal spot area) (10 × 10 mm^2), and b. solar cell area larger than the focal spot area (5.1 ×5.1 cm^2).

2.2.1. Focal Spot size > Solar Cell Area (Multi-junction /single-junction)

As known, the objective of the Fresnel lens is to concentrate solar irradiance onto a small solar cell area. Two types of solar cells are used to characterise the preliminary setup optic toward the ultrahigh system optically. Multi-junction (Azur Space 3C44A 10×10 mm^2) and single-junction polycrystalline solar cell are electrically measured. Figure 7. a and b show the electrical limits of multi-junction and single-junction solar cells in terms of I-V and power curves, respectively. At 1000 W/m^2, the introduction of the Fresnel Lens shows an increase in P_{max} by about 167 times and in I_{sc} by about 78 times for the multi-junction solar cell, as in Figure 7. a, whereas the growth in P_{max} and I_{sc} for the single-junction solar cell is by about 9 times and 34 times, respectively, as in Figure 7. b. The multi-junction solar cell is designed to perform optimally at 500 suns, where its efficiency, I_{sc}, V_{oc}, and FF 41.4%, 7.49A, 3.11A, and 89.6% (Azur Space Solar Power GMBH, 2014), respectively. The multi-junction solar cell's performance improves from where the primary optical component (Fresnel lens) at 77 suns and gradually increase to get closer to the optimum design condition. Hence, the multi-junction solar cell's V_{oc} increases significantly comparably with the single-junction solar cell.

The limitation of the single-junction solar cell, as not being design for concentration system, is the high series-resistance reflected on the drop of V_{oc} and power output compared with the multi-junction solar cell. The multi-junction solar cell can absorb many photons energy due to its wider bandgap energy (monolithic stack configuration), where less intrinsic losses occur, such as thermalisation loss, resulting in high cell efficiency.

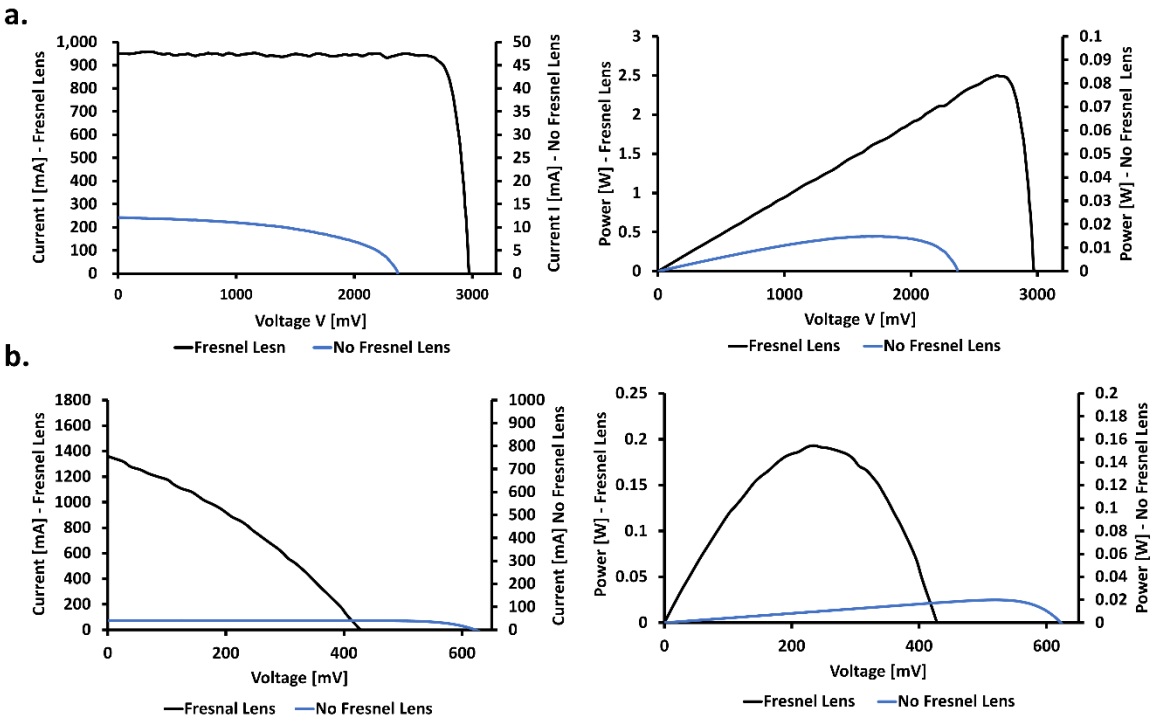

Figure 7 I-V and power curves limits with/ without Fresnel lens at 1000 W/m^2 of a. Azur Space multi-junction solar cell of 10×10 mm^2 and b. the single-junction solar cell of 10×10 mm^2.

Experimentally, the effective concentration ratio ($C_{eff,exp}$) can be characterised considering the measured I_{sc} with/without the Fresnel, as in Eq. 4.

$$C_{eff,exp} = \frac{I_{sc,concentrated}}{I_{sc,not\ concentrated}} \quad (4)$$

As in Figure 5, the theoretical effective optical concentration ratio was found to be 77 suns after the Fresnel, where the experimental effective concentration ratio was found to be 78 suns, which is agreeable with the theoretical effective concentration ratio by 98%. In anticipation of the optical concentration ratio, the geometrical concentration ratio could be approached either by considering only the Fresnel lens area ($0.0529m^2$) to the focal spot area ($A_{focal\ spot}$) ($0.0006157m^2$) or by considering the area of the Fresnel to the area of the solar cell and then apply the fractional concentration loss of 16.24%, as in Eq 5. The fractional concentration ratio only requires to be accounted for when the focal spot area is bigger than the solar cell, whilst the focal spot area matches the

solar cell (usually due to another funnel optic receiver) or is smaller than the solar cell (like in the case of 5.1 cm × 5.1 cm cell) then there is no fractional concentration loss.

$$C_g = \frac{A_{Fresnel}}{A_{focal\ spot}} = \frac{A_{Fresnel}}{A_{receiver}} \times \%C \quad (5)$$

Figure 8 shows the different value of effective irradiance incident on the solar cell (W) as secondary x-axis, the theoretical effective concentration ratio of the multi-junction and single-junction solar cell, as primary x-axis, and experimental effective concentration ratio of the multi-junction and single-junction solar cell, as the primary y-axis. A strong linear correlation exists between the theoretical and experimental effective concentration ratio for the multi-junction solar cell. The experimental results have shown higher results by 6% on average. This discrepancy may be due to the calibration of the helicon value to simulate the solar irradiance values. On the other hand, the single-junction solar cell could not compete with the multi-junction solar cell due to its design condition at 1 sun. Although at concentrated solar irradiance of 3.1 W (31 suns), the single-junction solar cell has shown the lowest difference by about 17%, this difference kept increasing gradually with a widening gap up to 6.2 W (62 suns), which could be elaborated as a bottleneck after the experimental effective concentration ratio decreased. On average, the difference between the theoretical and experimental effective concentration ratio is 39%. The single-junction solar cell's short circuit current can be used to indicate concentration ratio but the interest from these results is the scale of the overall power losses on the single-junction cell due to the out of working range concentration ratios. The ultimate aim is to test concentrator multi-junction cells at increasingly high and ultrahigh concentration ratios, beyond their designed operation. Hence, as a starting point, understanding the performance of the single-junction cell beyond its working concentration is a low-risk investigation. With increases in concentration ratio comes an increase in temperature of the cell, which when significantly higher than its recommended range (especially possible if there are hot spots due to concentrated irradiance distribution), can cause breakages. The single-junction cell would hence likely not cope with ultrahigh concentration ratios to aid the testing of the optics (via the short circuit current) but is a useful stepping stone in these preliminary investigations.

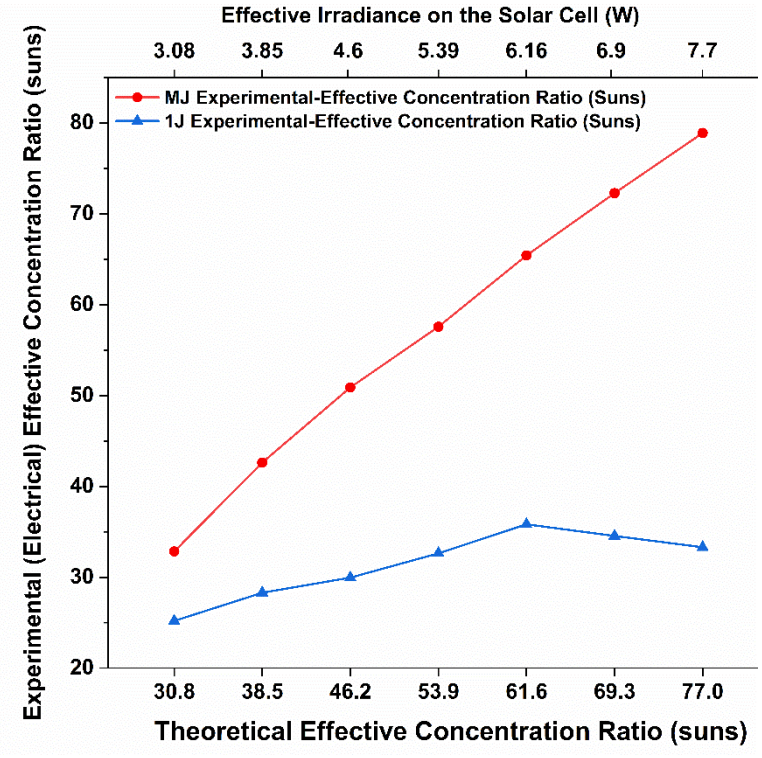

Figure 8 Theoretical and experimental effective concentration ratio for single- (1J) and multi-junction (MJ) solar cells where the experimental effective concentration ratio is calculated from the short circuit current increase of the cells.

2.2.2. Focal Spot size < Solar Cell Area (single-junction)

This section introduces the experimental optical characterisation for solar cell bigger than the produced focal spot size by the selected Fresnel lens. We have utilised Si polycrystalline single-junction (5.1 × 5.1 cm^2) solar cell. Figure 9 9 shows the I-V and power curves limits for with and without Fresnel lens. At 1000 W/m^2, the introduction of the Fresnel lens shows an increase in P_{max} by about four times and in I_{sc} by about 7 times. As highlighted in the previous section, this low performance is due to the high concentration ratio subjected to the solar cell surface inducing by that temperature.

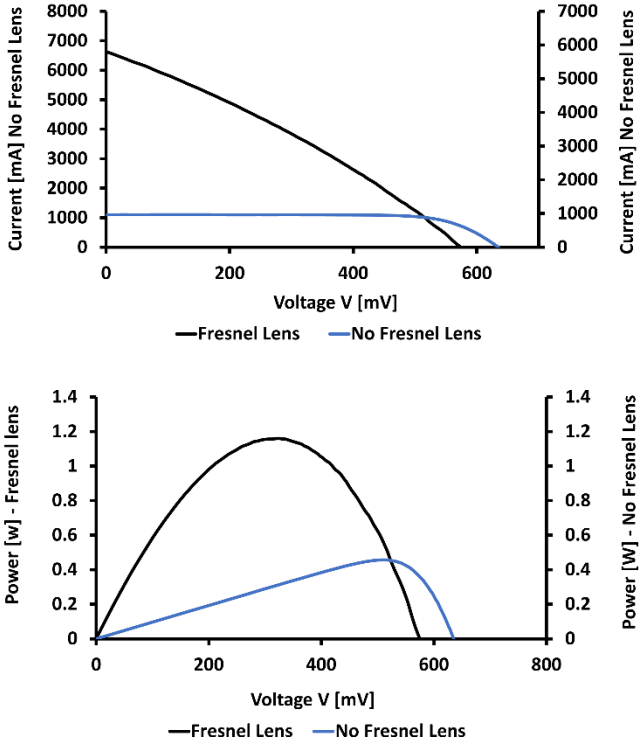

Figure 9 I-V and power curves limits with/ without Fresnel lens at 1000 W/m^2 of the single-junction solar cell of 5.1 × 5.1 cm^2

Both Eq .3 and Eq .4 were adopted to figure out the theoretical and effective concentration ratio. As known, the geometrical concentration ratio is the area of the Fresnel lens ($0.0529m^2$) to the area of the solar cell ($0.002601m^2$) resulting in 20 suns, as in Eq. 6.

$$C_g = \frac{A_{Fresnel}}{A_{receiver}} \quad (6)$$

Figure 10 shows the difference between the theoretical and experimental effective concentration ratio. We can observe that the experimental effective concentration ratio performs as a positive slope with the less difference at 19 W and after the difference is growing with increasing the solar irradiance on the cell. This logarithmic difference is noticeable where the curve is then flattened after 28.5 W. On average, the discrepancy between the experimental and the theoretical effective concentration ratio is by about 50%.

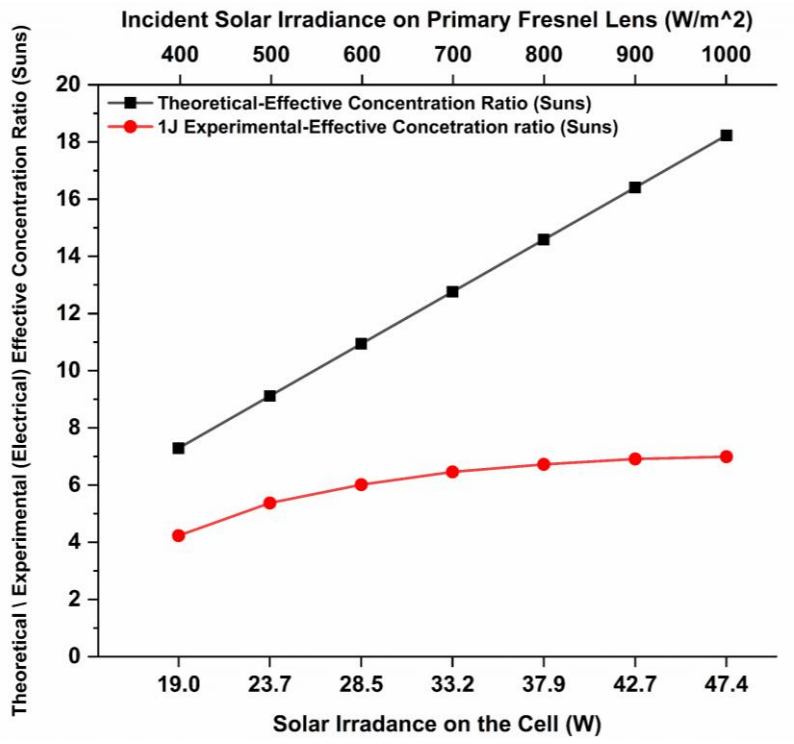

Figure 10 Theoretical and experimental effective concentration ratio for single-junction (1J) solar cells calculated from cell power output.

2.3. Effective Optical Efficiency Approach

To find out the effective optical efficiency ($\eta_{opt,eff}$), the electrical characterisation of the solar cell at different solar irradiance has been incorporated in Eq.7 to predict the effective optical efficiency considering the Fresnel lens efficiency (Module efficiency - η_{module}) concerning solar cell efficiency (η_{cell}). I_T/I_M terms in both Eq.1 and Eq.7 is only to express the subcell limits for the multi-junction cell.

$$\boldsymbol{\eta_{opt,eff}} = \frac{\boldsymbol{\eta_{module}}}{\boldsymbol{\eta_{cell}}} \times \frac{I_T}{I_M} \quad (7)$$

The module efficiency is the maximum electrical power output from the solar cell to the power input for the Fresnel lens, as in Eq. 8:

$$\boldsymbol{\eta_{module}} = \frac{\boldsymbol{Power_{max\,(V_{oc},I_{sc},F.F),concentrated}}}{\boldsymbol{J \times A_{Fresnel}}} \quad (8)$$

The theoretical module efficiency can be calculated by multiplying the optical efficiency of each component within the module and including any other forms of "stray light loss" such as the fractional loss discussed previously. This however must also take into account the intended wavelength range of the solar cell. The Fresnel lens optical transmissivity was measured to be an average of 89.63% for a spectral band compatible with a multi-junction solar cell of 400 -1800nm and in module efficiency of 91.1% for a spectral band matching up with single-junction solar cell of 350 – 1200 nm. As discussed, when this is multiplied by 16.24% (area of focal spot incident on cell) this becomes 14.6%. This optical efficiency (transmittance of Fresnel lens) would be the theoretical module efficiency if all of the light focused from the Fresnel lens fell incident within the cell area and the cell was designed as such to have a good fill factor under the effective concentration ratio. For the intended ultrahigh system, both of these factors will be significantly improved though substantial losses for each are anticipated due to alignment challenges (entendue challenges) and current available concentrator cells. Comparing the current setup with the ultrahigh setup will confirm experimentally the gain in such a complex ultrahigh system. However, the module efficiency was experimentally found to be 5% on average for the multi-junction solar cell and found to be 0.7% on average for the single-junction solar cell both of $10 \times 10\ mm^2$ surface area. The module efficiency for the multi-junction solar cell shows excellent stability within varying the DNI from 1000 $\frac{W}{m^2}$ to 400 $\frac{W}{m^2}$ in an interval of 100 $\frac{W}{m^2}$. On the other hand, the module efficiency for the single-junction solar cell was increased

gradually from 0.364% at 1000 $\frac{W}{m^2}$ to 1.17% at 400 $\frac{W}{m^2}$. For the case of $5.1 \times 5.1\ cm^2$ single-junction solar cell, the module efficiency was found to be 2.19% at 1000 $\frac{W}{m^2}$ and increased gradually to reach 5.36% at 400 $\frac{W}{m^2}$, resulting in average module efficiency of 3.28%.

The cell efficiency is the electrical output to the power input of the cell with concentration, which is driven from an Eq. 9:

$$\eta_{cell} = \frac{Power_{max\,(V_{OC}, I_{SC}, F.F),concentrated}}{Radient\ flux\ on\ the\ target\ area\ ((J \times A_{Fresnel}) \times \%T \times \%C)} \quad (9)$$

Experimentally, the power output for both single-junction and multi-junction solar cells was measured to compute the cell efficiency. As a result, the cell efficiency of $10 \times 10\ mm^2$ multi-junction solar cell was found to be 33.5% on average, with excellent consistency with altering the DNI input value. In contrast, the single-junction solar cell of $10 \times 10\ mm^2$ surface area showed a cell efficiency increasing progressively from 2.5% at a solar simulator irradiance of 1000 $\frac{W}{m^2}$ to 8% at a solar simulator irradiance of 400 $\frac{W}{m^2}$. Also, the single-junction solar cell of $5.1 \times 5.1\ cm^2$ surface area represented a cell efficiency increasing steadily from 2.4% at 1000 $\frac{W}{m^2}$ to 5.88% at 400 $\frac{W}{m^2}$.

As in Eq. 1, the theoretical optical efficiency of both $10 \times 10\ mm^2$ single- and multi-junction solar cell is found to be 14.6% due to accounting for the concentration fractional loss. Experimentally, the effective optical efficiency of both $10 \times 10\ mm^2$ single- and multi-junction solar cell leads to an exact similar result with the theoretical one, as in Eq.7. With varying the DNI value, the multi-junction solar cell showed consistency in both cell and module efficiencies resulting in a constant optical efficiency. On the other hand, the single-junction solar cell showed a gradual increase in both cells in module efficiencies, causing a continuous optical efficiency with changing the DNI value. In the case of $5.1 \times 5.1\ cm^2$ single-junction solar cell, the theoretical and experimental optical efficiency is found to be 91.1% as the fractional loss discarded. Both cell and module efficiencies raised steadily, resulting in a continuous optical efficiency altering the DNI value. Compared to the experimental one, the high theoretical effective optical efficiency is because the single-junction solar cell is designed to cope with 1 sun. The overall study parameters and results are summarised in Table 1.

Table 1 Summarise the geometric concentration, theoretical/experimental optical concentration ratio, and the optical efficiency in every testing scenario at 1000 $\frac{W}{m^2}$.

Solar Cells	Geometrical concentration ratio (x)(Cg)	Theoretical Optical Concentration ratio (suns) ($C_{th\ and}\ C_{eff,th}$)	Experimental Optical Concentration ratio (suns) ($C_{eff,exp}$)	Theoretical Optical Efficiency (%) ($\eta_{opt,th}$)	Effective Optical Efficiency (%) ($\eta_{opt,eff}$)
$1 \times 1\ cm^2$ (1J)	529	77	33	14.6	14.6
$5.1 \times 5.1\ cm^2$(1J)	20	18	7	91.1	91.1
$1 \times 1\ cm^2$ (MJ)	529	77	79	14.6	14.6

Although the concentration ratio value is far from the ultrahigh concentration limits, these results are an important step towards carrying out the full ultrahigh concentration setup experiment. This paper is focused on evaluating the optical components (Fresnel lens) individually, and the performance of the concentrator multi-junction cell in these poorer conditions to have a concrete reference performance for the full ultrahigh system.

Table 2 is listing all the detailed equations previously in three sections geometrical concentration, theoretical calculation, and experimental calculation. The number of equations in the table is correspondent to the number of equations in the paper.

Table 2 Summary for the used equations to solve for the optical concentration ratio and optical efficiency theoretically and experimentally.

Number of Equation	Name of Equation (unit)	Equation
	Geometrical Concentration	
5	Geometrical concentration for focal spot larger than the cell (x)	$C_g = \frac{A_{Fresnel}}{A_{focal\ spot}} = \frac{A_{Fresnel}}{A_{receiver}} \times \%C$
6	Geometrical concentration ratio for solar cell larger than the focal spot (x)	$C_g = \frac{A_{Fresnel}}{A_{receiver}}$
	Theoretical Calculations	
1	Theoretical Optical Efficiency (%)	$\eta_{opt,th} = \frac{(\mathrm{J} \times A_{receiver}) \times \%T \times C_g \times \%C}{(J \times A_{Fresnel})} \times \frac{I_T}{I_M}$
2	Theoretical Optical Concentration ratio (suns)	$C_{th} = \eta_{opt,th} \times C_g$
3	Theoretical effective concentration ratio (suns)	$C_{eff,th} = \frac{J \times C_g \times \eta_{opt,th}}{1000} = \frac{J \times A_{Fresnel} \times \%T}{A_{receiver} \times 1000}$
	Experimental Calculations	
4	Effective concentration ratio (suns)	$C_{eff,exp} = \frac{I_{sc,concentrated}}{I_{sc,not\ concentrated}}$
7	Effective optical efficiency (%)	$\eta_{opt,eff} = \frac{\eta_{module}}{\eta_{cell}} \times \frac{I_T}{I_M}$
8	Module efficiency (%)	$\eta_{module} = \frac{Power_{max\ (V_{oc}, I_{sc}, F.F),concentrated}}{J \times A_{Fresnel}}$
9	Cell efficiency (%)	$\eta_{cell} = \frac{Power_{max\ (V_{oc}, I_{sc}, F.F),concentrated}}{Radient\ flux\ on\ the\ target\ area\ ((J \times A_{Fresnel}) \times \%T \times \%C)}$

3. Theoretical Perspective Toward Ultrahigh CPV System

As a primary optical component toward the full UHCPV system as in (Shanks et al., 2018), the refractive optic (Fresnel lens) is characterised theoretically and experimentally. This Fresnel lens is 1 of 4 primary Fresnel lens optics exactly the same, which would make up the entry aperture (primary optic) for an ultrahigh CPV system of concentration ratio > 3000 suns. In this section, the subsequent optics, which are flat reflective mirror and tertiary optics on the top of the solar cell, are theoretically discussed, accounting only for three optical stages starting with the Fresnel lens to the flat plain reflective optical mirror ending with the tertiary optic. Due to the fractional concentration loss, significant loss occurs in the optical performance when compromised electrically, as systematically explained in the previous section. Incorporating more than one optic in the CPV system results in increasing the concentration ratio through minimised sunrays divergence. There will likely still be some loss and hence the optical efficiency of 14.6% due to the fractional loss is considered as the worst-case scenario through which the UHCPV system will be theoretically analysed and discussed. Certainly, the fractional loss would increase with increasing the concentration ratio. Checking the irradiance distribution of the Fresnel lens would reflect an increase in the fractional loss If the short-circuit current given here gave a concentration value significantly higher than the fractional loss indicated then the majority of the irradiance was actually focused on the inner area of the focal spot – where the 1cm cells are placed, which would be important to know for the ultrahigh system. Still, the ultrahigh system is strongly influenced by alignment, manufactured optical materials, the temperature of optics and incidence source light (divergence angle).

In the ultrahigh CPV system design, four or three optical interfaces will be incorporated to accomplish an ultrahigh concentration ratio configuration. In the case of four optical stages, the sunrays will be refracted from the Fresnel lens into the flat reflective secondary mirror, which reflects concentrated sun rays into the third stage flat central mirror. Afterwards, the third stage flat central mirror will reflect the concentrated rays into the low refractive tertiary optic as a final optical stage. Although this number of optics in one system will add to the complexity of the fabrication and challenge the accuracy and alignment of the system, 1 of these optical stages is a flat mirror which should have minimum light divergence effects if of high quality.These optical stages will aid the system at which the convergence angle is minimised (less fractional concentration loss), resulting in increased concentration ratio. Inherently, a minimum light divergence (the maximum angle from the furthest incident rays from the normal axis to arrive at the focal spot) has a smaller acceptance angle, adding to the tracking system load and accuracy. In the UHCPV system, the concentrated rays would still not converge enough into the solar cell area, resulting in a reduction in the optical efficiency and hence in the optical concentration ratio. Although the UHCPV system aims to incorporate smaller multi-junction solar cells for higher geometrical concentration ratio, less heat generation, and higher cell efficiency, the CPV system is challenged in design and alignment accuracy. Refractive tertiary optics is suggested and implemented on the top surface of the solar cell. Although tertiary optics would decrease the optical efficiency also, tertiary optics improve the acceptance angle and the uniformity of irradiance distribution

3.1 Theoretical Review of Secondary Mirror Coatings

The UHCPV system consists of Fresnel lens, as primary refractive optic, reflective mirror, as a secondary optic, and a tertiary centre optic, as final refractive optic attached on the solar cell. The secondary reflective mirror will be interpolated for four different metallic coatings: UV aluminium mirror, enhanced aluminium mirror, silver mirror, and gold mirror. These secondary mirrors optical efficiency (Reflectance %) are retrieved from the NEWPORT Corporation (Newport Corporation, n.d.) for broadband metallic mirrors (Borofloat 33), which operates well over a very wide-ranging of spectral wavelength with relatively insensitive to angle of polarisation and incident. Regarding tertiary centre optic, the transmittance (%) performance of SK-700 material was retrieved from (Leem and Yu, 2012)(Shanks et al., 2018). The retrieved data will be integrated as a consecutive optic to the Fresnel lens to theoretically evaluate the optical efficiency and optical concentration ratio for a quarter of the system. The integration of the tertiary centre has dropped the optical efficiency due to the scattering losses at the top surface of the tertiary in the absence of the antireflective coating(Bruns et al., 2016) and the absorbance properties of the tertiary itself..

Figure 11 shows the optical performance, optical efficiency as a primary y-axis of the Fresnel lens (SOG) itself, of SK-700 dependent on the performance of the Fresnel lens, and the four types of metallic coating dependent on the performance of both Fresnel lens and SK-700, as in Eq. 10.

$$\eta_{opt,th} = \eta_{Fresnal\ lens} \times \eta_{metallic\ coating\ (UV\ aluminum,\ Enhanced\ Aluminum,\ Silver,\ and\ Gold)} \times \eta_{SK-700} \quad (10)$$

The optical efficiency, in Figure 11, is showing the losses for three optical stages, first the Fresnel lens material absorption and scattering, second the mirror's coatings reflectivity, and third the tertiary optics absorption and scattering. Hence, the three stages' performance would produce the final optical efficiency and concentration ratio for only ¼ of the system, when all 4 lenses and mirrors are in place the concentration would be × 4 (as all focal spots from each of the 4 Fresnel lenses are redirected via flat mirrors towards the centre (Shanks et al., 2018). Achieving high optical efficiency for 3 mm × 3 mm cell and optics setup as its maximum geometrical concentration ratio would become 23,511x, which it seems unlikely to be reached in real-life testing conditions within the current available optics and manufacturing. Given the fractional loss optical efficiency of 14.6%, the system optical efficiency would be 3433x, which is still within the target of the design of >3000 suns. However, such an analysis is given to illustrate how considerable the effect of the final receiver size on the concentration ratio.

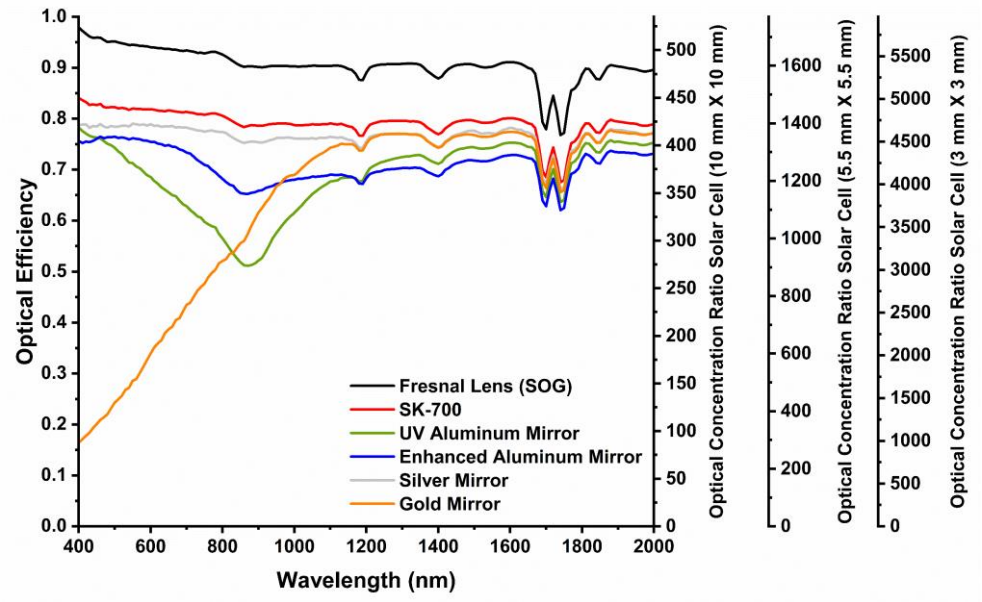

Figure 11 Theoretical optical efficiency with wavelength (400 – 2000 nm) for four different reflective mirrors as a secondary optical stage associated with both the Fresnel lens and the SK-700. The optical concentration ratio computed relying on a solar cell area of 10 × 10 mm^2, 5.5 × 5.5mm^2, and 3 × 3 mm^2 as a final stage and no fractional losses.

On average, the optical efficiency of the Fresnel lens and SK-700 extrapolated from Figure 11 to be 79%. Also, the optical efficiency has been 69%, 71%, 77%, and 63% for UV aluminium mirror, enhanced aluminium mirror, silver mirror, and gold mirror incorporated with Fresnel lenses and SK-700, respectively. The highest optical efficiency is for silver coating mirror (>96% from 480-1100 nm; >98.5 for >1.1 nm), which is better suited to multi-junction solar cell (∼350nm – 1600nm). However, the silver coating deteriorates when exposed to extreme metrological conditions, especially under concentrated sunrays. NEWPORT Corporation utilises silver film of low emissivity, which is entirely encapsulated by a dielectric stack of multilayer to avoid oxidisation. The silver coating exhibited an excellent reflectivity performance on IR wavelength range while maintaining a proper performance in both visible and near IR. The most inferior performance is for gold mirror (> 96% from 650-1700 nm; > 98% for > 1.7 nm) because its ideal for application requiring reflectance near IR and for the onward IR, an overcoat of a multilayer dielectric provides preservation to the gold from the outside weather conditions. In the case of the enhanced aluminium mirror, the average reflectivity is > 93% from 450-700 nm, and a dielectric stack of the multilayer is applied over the aluminium surface to increase reflectivity and enhance durability. An enhanced aluminium mirror is very suitable for the application required spectral band for visible and near-infrared. UV enhanced mirror has an average reflectivity of 90% from 250-600 nm. Also, UV enhanced mirror is proper for most applications due to its durability, which is enhanced by applying dielectric overcoating to avoid oxidisation of the metal.

Figure 11 11 shows the optical concentration ratio for a quarter of the system a secondary y-axis for where the first secondary y-axis, second secondary y-axis, and third secondary y-axis is based on a geometrical concentration ratio for solar cell area of (10 × 10 mm^2), (5.5 × 5.5 mm^2), and (3 × 3 mm^2), respectively. On average, the optical concentration ratio has been computed for a spectral band from 400 – 2000 nm, as in Table 3 and as plotted in Figure 12.

Table 3 The data extrapolated from Figure 11 for four different types of metallic coatings on average across a wavelength range of 400 – 2000 nm for a quarter of the system.

Solar cell Area (mm)	**The optical concentration ratio (suns)**			
	UV Aluminum Mirror	Enhanced Aluminum Mirror	Silver Mirror	Gold Mirror
10 × 10	364	376	405	333
`5.5 × 5.5	1202	1239	1334	1100
3 × 3	4040	4166	4500	3699

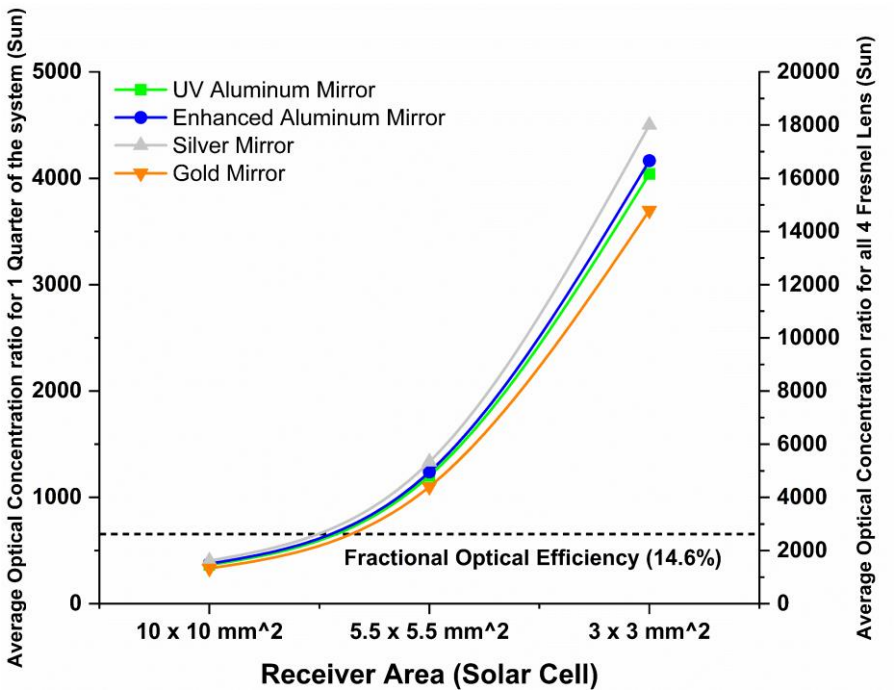

Figure 12 Optical concentration ratio plotted from Table 3 for three sizes of the final receiver (solar cell) and for four types of metallic coatings associated with the tertiary optic (SK-700) and the Fresnel lens.

For the entire system and given the geometrical concertation ratio for the selected primary optical stage, ultrahigh concentration ratio >3000 suns is not achievable for a receiver area of $10 \times 10\ mm^2$ since the optimum theoretical concentration ratio for the silver mirror compared to others is 1620 suns. Indeed, the solar cell area of $5.5 \times 5.5\ mm^2$ and $3 \times 3\ mm^2$ is capable of attaining the ultrahigh concentration ratio. The optical losses are more likely to occur due to further transmittance and reflectiveness loss. Also, the amount of the accumulated heat at the focal spot due to the ultrahigh concentration ratio might induce other losses when compromising the optical performance electrically as the electrical performance deteriorates if no suitable cooling mechanism is in-place. The secondary reflective mirror function is to minimise the light divergence, and the tertiary optics role is to funnel as much of the focal point light and concentrate it further to the cell size, hence minimising the geometrical fractional loss. The tertiary optic only reduces fractional loss but add some absorption/scattering to the concentrated light. So, the added dashed line in Figure 12 gives a theoretical estimate of the minimum concentration ratio for the system. The aim is to build a prototype that falls within the solid lines and the dashed lines. Given the limits of ultrahigh concentration ratio of > 3000 suns and the calculated theoretical concentration ratio based on the selected optical mirror, the range of optical losses differ depending on the optical stages and their optical performance for solar cell area of $5.5 \times 5.5\ mm^2$ and $3 \times 3\ mm^2$ wherein our case and based on the selected optics. The detailed losses based on the performance of the coated reflective mirror have listed in Table 4.

Table 4 The room of optical concentration ratio loss based on the selected optics and the metallic coating typed for the secondary reflective mirror and solar cell area of $5.5 \times 5.5\ mm^2$ and $3 \times 3\ mm^2$

Solar cell Area (mm)	The range of optical concentration ratio losses (%)			
	UV Aluminium Mirror	Enhanced Aluminium Mirror	Silver Mirror	Gold Mirror
`5.5 × 5.5	37.6%	39.4%	43.8%	31.8%
3 × 3	81.4%	81.9%	83.3%	79.7%

4. Conclusions

The indoor optical characterisation is adopted to characterise the optical performance of the Fresnel lens theoretically and effectively. This approach allows simple measurements to estimate the effective optical efficiency and effective concentration ratio, especially in a concentrated photovoltaic system (CPV). From this optical characterisation, we can extract that the optical performance decay significantly due to the fractional concentration loss and the designing conditions of single-junction solar cells. Also, the multi-junction solar cell

has shown minimal inconsistency in the experimental optical characterisation compared to the single-junction solar cells, resulting in a discrepancy of 2% at 7.7 W and 6% on the average cross a concentrated solar irradiance on the cell from 3.1 – 7.7 W. The theoretical analysis of the overall optical components in the UHCPV emphasised the optical losses and aspects that challenge the system to reach a concentration ratio > 3000 suns. Four different metallic coatings for the reflective secondary mirror have been analysed considering the range of optical losses to still achieve the ultrahigh concentration ratio and balance that with the correlation between the solar cell size and the primary optic size (geometrical concentration ratio).

5. Declaration of competing interest

The authors declare that they have no known competing financial interests or personal relationships that could have appeared to influence the work reported in this article.

Acknowledgement

M.A would like to duly acknowledge the financial support from the Saudi Arabia Culture Bureau in the U.K. As well, the Ph.D. scholarship of A.A funded by Newton-Mosharafa Fund (UK-Egypt partnership) is acknowledged. The funders have no role in study design data collection, or preparation of the manuscript.

References

AlFalah, G., Maatallah, T.S., Alzahrani, M., Al-Amri, F.G., 2020. Optimisation and feasibility analysis of a microscale pin-fins heat sink of an ultrahigh concentrating photovoltaic system. International Journal of Energy Research 44, 11852–11871. https://doi.org/10.1002/er.5826

Alzahrani, M., Baig, H., Shanks, K., Mallick, T., 2020. Estimation of the performance limits of a concentrator solar cell coupled with a micro heat sink based on a finite element simulation. Applied Thermal Engineering 115315. https://doi.org/10.1016/j.applthermaleng.2020.115315

Alzahrani, M., Roy, A., Shanks, K., Sundaram, S., Mallick, T.K., 2021a. Graphene as a pre-illumination cooling approach for a concentrator photovoltaic (CPV) system. Solar Energy Materials and Solar Cells 222, 110922. https://doi.org/10.1016/j.solmat.2020.110922

Alzahrani, M., Shanks, K., Mallick, T.K., 2021b. Advances and limitations of increasing solar irradiance for concentrating photovoltaics thermal system. Renewable and Sustainable Energy Reviews 138, 110517. https://doi.org/10.1016/j.rser.2020.110517

Alzahrani, M.M., Roy, A., Sundaram, S., Mallick, T.K., 2021. Investigation of Thermal Stress Arising in a Graphene Neutral Density Filter for Concentrated Photovoltaic System. Energies 14, 3515. https://doi.org/10.3390/en14123515

Azur Space Solar Power GMBH, 2014. Enhanced Fresnel Assembly - EFA Type: 3C42A – with 10x10mm^2 CPV TJ Solar Cell Application: Concentrating Photovoltaic (CPV) Modules 0–4.

Bruns, S., Vergöhl, M., Zickenrott, T., Bräuer, G., 2016. Deposition of abrasion resistant single films and antireflective coatings on sapphire. Surface and Coatings Technology 290, 10–15. https://doi.org/10.1016/j.surfcoat.2015.11.011

Canavarro, D., Chaves, J., Collares-Pereira, M., 2013. New second-stage concentrators (XX SMS) for parabolic primaries; Comparison with conventional parabolic trough concentrators. Solar Energy 92, 98–105. https://doi.org/10.1016/j.solener.2013.02.011

Chemisana, D., Vossier, A., Pujol, L., Perona, A., Dollet, A., 2011. Characterisation of Fresnel lens optical performances using an opal diffuser. Energy Conversion and Management 52, 658–663. https://doi.org/10.1016/j.enconman.2010.07.044

Daneshazarian, R., Cuce, E., Cuce, P.M., Sher, F., 2018. Concentrating photovoltaic thermal (CPVT) collectors and systems: Theory, performance assessment and applications. Renewable and Sustainable Energy Reviews 81, 473–492. https://doi.org/10.1016/j.rser.2017.08.013

Dreger, M., Wiesenfarth, M., Kisser, A., Schmid, T., Bett, A.W., 2014. Development and investigation of a CPV module with cassegrain mirror optics. AIP Conference Proceedings 1616, 177–182. https://doi.org/10.1063/1.4897055

El-Gahouchi, M., Aziziyan, M.R., Arès, R., Boucherif, A., 2020. Optimised duplicated-junction solar cells: An innovative approach for energy harvesting at ultra-high concentrations. p. 020003. https://doi.org/10.1063/5.0032136

Fernández, E.F., Almonacid, F., Rodrigo, P.M., Pérez-Higueras, P., 2017. CPV Systems. McEvoy's Handbook Photovoltic, pp. 931–985.

Ferrer-Rodríguez, J.P., Fernández, E.F., Almonacid, F., Pérez-Higueras, P., 2016. Optical design of a 4-off-axis-unit Cassegrain ultra-high concentrator photovoltaics module with a central receiver. Optics Letters 41, 1985. https://doi.org/10.1364/ol.41.001985

Fu, L., Leutz, R., Annen, H.P., 2010. Secondary optics for Fresnel lens solar concentrators, in: Winston, R., Gordon, J.M. (Eds.), International Society for Optics and Photonics. p. 778509. https://doi.org/10.1117/12.860438

Gordon, J.M., Feuermann, D., Young, P., 2008. Unfolded aplanats for high-concentration photovoltaics. Optics Letters 33, 1114. https://doi.org/10.1364/OL.33.001114

Hornung, T., Steiner, M., Nitz, P., 2011. Estimation of the influence of Fresnel lens temperature on energy generation of a concentrator photovoltaic system. AIP Conference Proceedings 1407, 97–100. https://doi.org/10.1063/1.3658303

Jing, L., Liu, H., Zhao, H., Lu, Z., Wu, H., Wang, H., Xu, J., 2012. Design of novel compound fresnel lens for high-performance photovoltaic concentrator. International Journal of Photoenergy 2012. https://doi.org/10.1155/2012/630692

Leem, J.W., Yu, J.S., 2012. Superhydrophilic Sapphires for High- Performance Optics. Optics Express 20, 769–773.

Martinez Antón, J.C., Vázquez Moliní, D., Muñoz de Luna, J., Gómez Pedrero, J.A., Fernández-Balbuena, A.Á., 2011. Method for the characterization of Fresnel lens flux transfer performance. Optical Fabrication, Testing, and Metrology IV 8169, 81690E. https://doi.org/10.1117/12.896870

Miñano, J.C., Benítez, P., Zamora, P., Buljan, M., Mohedano, R., Santamaría, A., 2013. Free-form optics for Fresnel-lens-based photovoltaic concentrators. Optics Express 21, A494. https://doi.org/10.1364/oe.21.00a494

Muñoz-Cerón, E., Miñano, J.C., Benítez, P., Almonacid, G., Buljan, M., 2012. On-site measurement of limiting subcell in multijunction solar devices. pp. 157–160. https://doi.org/10.1063/1.4753857

Newport Corporation, n.d. Neutral Density Filter Selection Guide [WWW Document]. URL https://www.newport.com/g/neutral-density-filter-selection-guide (accessed 3.1.20).

Sansoni, P., Francini, F., Fontani, D., 2007. Optical characterisation of solar concentrator. Optics and Lasers in Engineering 45, 351–359. https://doi.org/10.1016/j.optlaseng.2005.02.009

Shanks, K., Ferrer-rodriguez, J.P., Fernández, E.F., Almonacid, F., 2018. A > 3000 suns high concentrator photovoltaic design based on

multiple Fresnel lens primaries focusing to one central solar cell. Solar Energy 169, 457–467. https://doi.org/10.1016/j.solener.2018.05.016
Shanks, K., Senthilarasu, S., Mallick, T.K., 2016. Optics for concentrating photovoltaics: Trends, limits and opportunities for materials and design. Renewable and Sustainable Energy Reviews 60, 394–407. https://doi.org/10.1016/j.rser.2016.01.089
Sharaf, O.Z., Orhan, M.F., 2015. Concentrated photovoltaic thermal (CPVT) solar collector systems: Part I – Fundamentals, design considerations and current technologies. Renewable and Sustainable Energy Reviews 50, 1500–1565. https://doi.org/10.1016/j.rser.2015.05.036
Suns, U.L.C., Fernández, E.F., Seoane, N., Almonacid, F., García-loureiro, A.J., 2019. Vertical-Tunnel-Junction (VTJ) Solar Cell for 40, 2018–2021.
Tang, R., Liu, X., 2011. Optical performance and design optimisation of V-trough concentrators for photovoltaic applications. Solar Energy 85, 2154–2166. https://doi.org/10.1016/j.solener.2011.06.001
Tang, R., Wang, J., 2013. A note on multiple reflections of radiation within CPCs and its effect on calculations of energy collection. Renewable Energy 57, 490–496. https://doi.org/10.1016/j.renene.2013.02.010
Tawalbeh, M., Al-Othman, A., Kafiah, F., Abdelsalam, E., Almomani, F., Alkasrawi, M., 2021. Environmental impacts of solar photovoltaic systems: A critical review of recent progress and future outlook. Science of The Total Environment 759, 143528. https://doi.org/10.1016/j.scitotenv.2020.143528
Valera, A., Fernández, E.F., Rodrigo, P.M., Almonacid, F., 2019. Feasibility of flat-plate heat-sinks using microscale solar cells up to 10,000 suns concentrations. Solar Energy 181, 361–371. https://doi.org/10.1016/j.solener.2019.02.013
Victoria, M., Askins, S., Herrero, R., Domínguez, C., Nuñez, R., Antón, I., Sala, G., 2016. Measuring primary lens efficiency: A proposal for standardisation. AIP Conference Proceedings 1766. https://doi.org/10.1063/1.4962123
WACOM ELECTRIC LTD [WWW Document], 2021. URL https://wacom-ele.co.jp/en/ (accessed 7.1.21).
Wang, H., Huang, J., Song, M., Hu, Y., Wang, Y., Lu, Z., 2018. Simulation and experimental study on the optical performance of a fixed-focus Fresnel lens solar concentrator using polar-axis tracking. Energies 11. https://doi.org/10.3390/en11040887
Wiesenfarth, M., Steiner, M., Wolf, J., Schmidt, T., Bett, A.W., 2014. Investigation of different fresnel lens designs and methods to determine the optical efficiency. AIP Conference Proceedings 1616, 97–101. https://doi.org/10.1063/1.4897037
Winston, R., Miñano, J.C., Benítez, P., 2005. APPLICATIONS TO SOLAR ENERGY CONCENTRATION, in: Nonimaging Optics. Elsevier, pp. 317–394. https://doi.org/10.1016/B978-012759751-5/50013-0